VOLUME 39(1996), 4, 943–949
TRIBOLOGY TRANSACTIONS

Accelerated High Speed Water Erosion Test for Concrete Wear Debris Analysis©

ANDREAS W. MOMBER and RADOVAN KOVACEVIC
University of Kentucky
Center for Robotics and Manufacturing Systems
Lexington, Kentucky 40506

This paper contains investigations of wear particles generated during the erosive wear of four different concrete mixtures by high velocity water flow at velocities of about 700 m/s. The wear particles were collected, dried and analyzed by sieve experiments. Based on the sieve analysis, specific surface and average grain diameter of the particle samples were estimated. Using simple comminution relations, the specific crack length of every sample is calculated. It is shown that all estimated parameters exhibit a strong relationship to characteristic material properties, such as compressive strength, Young's modulus, and absorbed fracture energy. It was found by regression analysis that the average debris wear size can be effectively characterized by the absorbed fracture energy of the concrete sample. It is concluded that these relations are the result of different paths of fracture propagation through the materials during the generation of a microcrack network.

KEY WORDS

Wear and Failure, Erosive Wear Mechanisms, Materials, Properties and Tribology, Marine Tribology

Presented as a Society of Tribologists and Lubrication Engineers paper at the ASME/STLE Tribology Conference in San Francisco, California, October 13–17, 1996
Final manuscript approved August 25, 1995

INTRODUCTION

Since concrete is used for marine and hydraulic structures, pipe coatings and channel walls, its wear due to the attack of fast flowing water is a problem (*1*). The first systematic investigations on the resistance of concrete against wear in marine structures were carried out in the 1940s (*2*). Investigations carried out in the fields of water flow erosion, cavitation and abrasion have been reviewed in Refs. (*3*), (*4*).

Momber et al. (*3*)–(*10*) investigated the influences of interfaces, cracks, and inclusions on the failure of brittle multiphase materials due to fast flowing water attack at velocities up to 450 m/s. The predominant mechanisms of the material failure are propagation and intersection of pre-existing microcracks. It was found that the destruction process due to the water flow is introduced in the interface between the matrix and inclusions which are characterized by a high degree of porosity and pre-existing microcracks. The water is pressurized inside a crack; this leads to forces acting on the crack wall surfaces. If the generated stresses exceed critical material values, e.g., critical stress intensity factor, the crack starts to grow. The crack growth is controlled by the interaction between crack and aggregate grains. It was experimentally shown that inclusions in the material may act as crack arrestors and energy dissipators (*8*). The intersection of several single cracks leads to a macroscopical material removal. The model is illustrated in Fig. 1. In advanced versions of the phenomenological model, a computer-based simula-

NOMENCLATURE

a,b,c = regression parameters
C_M = sound velocity in the target material
d = sieve width
d_{AV} = average wear particle diameter
l_0 = maximum sieve width
d_U = minimum sieve width
E = Young's modulus
G = absorbed fracture energy
K = compressive strength
K_{Ic} = fracture toughness
l_{cr} = specific crack length
p = applied pump pressure
S_{SP} = specific surface of a grain sample
v_{fl} = water flow velocity
V_M = removed material volume
$\dot{\varepsilon}$ = strain rate
μ = nozzle efficiency parameter
ρ = water density
ρ_M = target material density
ψ = particle shape parameter

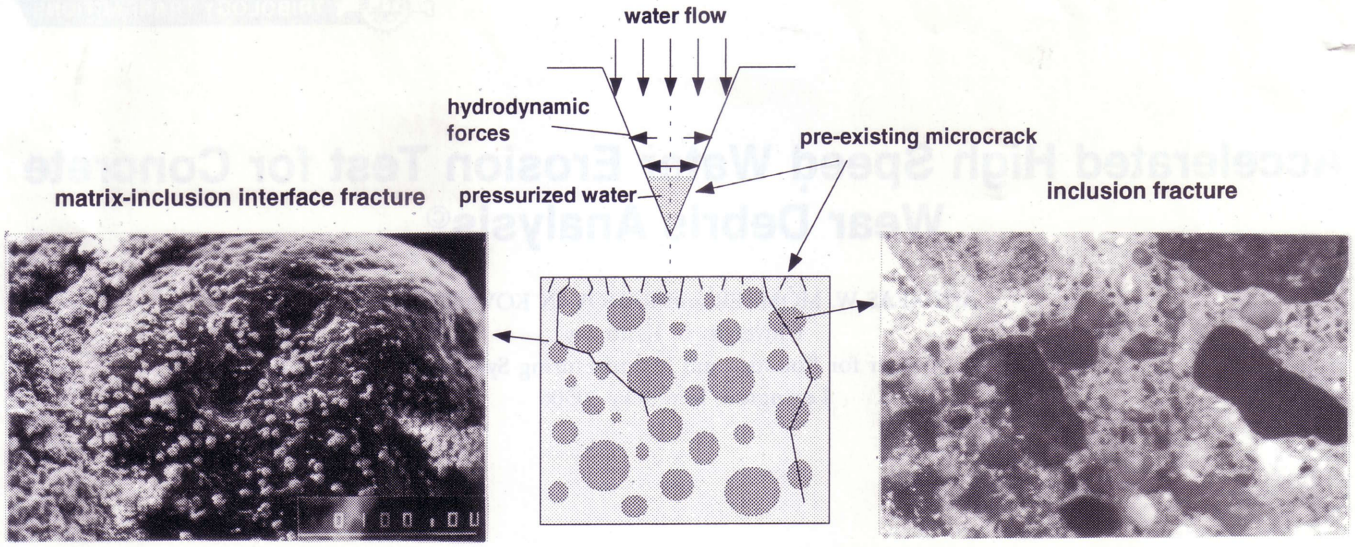

Fig. 1—High speed water flow erosion model for concrete.

tion of the fluid dynamics inside a microcrack (*4*) and a fracture mechanics model for the characterization of the erosion process (*10*) are presented.

The main conclusion from these investigations is that the erosive wear of concrete and similar semi-brittle, multiphase materials, such as motars, rocks, and minerals, may be interpreted as a fracture mechanics process which deals with the generation, propagation and intersection of cracks. The generated wear debris may be considered to be a result of these processes and contain some information on the process. There may be, in particular, relations between the size of the wear particles and the structure of the generated microcrack network in the materials. Generally, in terms of wear, the essential requirement is to determine its extent and its physical basics. With regard to wear particles, the scope for establishing their characteristics resides in determining their quantity, size, composition and morphology (*11*). Figure 2 shows some relationships between wear and wear particle characteristics.

It is the objective of this paper to relate the size of the generated wear particles to the fracture process in the material.

INVESTIGATED MATERIALS AND EXPERIMENTAL SETUP

Investigated Materials

Four different concrete mixtures were designed and investigated to analyze the wear particles. Five cylindrical specimens (30.48 cm in length and 15.24 cm in diameter) of each mixture were cast. The aggregates consist of two types, such as quartzite grains as coarse aggregates and river sand as fine aggregates. Both types of aggregates are mixed in different ratios to obtain a different fineness of the final aggregate mixture for the four concretes, as shown in Table 1. These final aggregates were mixed with the binding agent (cement) in a ratio 2.24:1. The water-cement ratio was varied according to Table 1. After mixing, the compositions were cured and hardened for 28 days under water. After hardening, three cylindrical specimens of every mixture were tested. The compressive strength was estimated according to the ASTM Standard C 39 and the Young's modulus was measured as the static chord modulus according to the ASTM Standard C 469. The absorbed fracture energy was estimated by integrating the area under the stress-strain curves of every material between zero and the ultimate strain. Therefore, one specimen of every mixture was loaded and unloaded 11 times to obtain the stress-strain relation. The experimentally estimated stress-strain curve was fitted by a second-order polynomial. The results of these measurements are given in Table 1.

Testing Equipment and Performance

The high speed water flow attack was simulated by a water jet impact with a velocity of 700 m/s. The flow velocity was calculated from the pressure of the pumping unit according to:

$$v_{fl} = \mu \cdot \sqrt{\frac{2 \cdot p}{\rho}} \qquad [1]$$

Here, v_{fl} is the water flow velocity and μ is a nozzle efficiency parameter, which is $\mu = 0.95$ for the given pump pressure

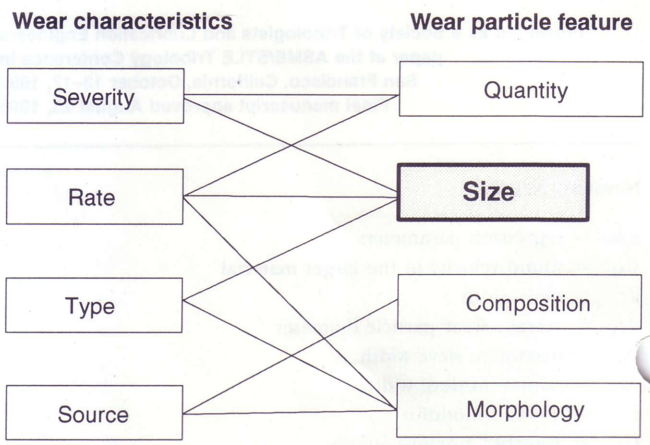

Fig. 2—Relations between wear characteristics and wear particle features (*11*).

TABLE 1—PROPERTIES OF THE USED CONCRETE MIXTURES

CONCRETE MIXTURE	AGGREGATE*/ CEMENT**	SAND*** (%)	WATER/ CEMENT	E (GPa)	K (MPa)	G (MJ/m^3)	ρ_M (kg/m^3)
1	2.24	80	0.85	10.7	4.0	1.5	1,962
2	2.51	70	0.71	24.1	12.5	7.9	2,135
4	2.25	50	0.38	34.3	34.2	40.9	2,275
5	2.26	40	0.32	42.3	41.1	47.6	2,343

*coarse aggregate: crushed limestone (maximum grain size 19 mm)
fine aggregate: river sand (maximum grain size 4.7 mm)
**Portland Cement, Type I
***amount of river sand in the aggregate mixture

(*12*). Further, p is the pump pressure and ρ is the water density. More details of water jet generation, structure and action are found in Ref. (*13*).

The high velocity water jet unit consists of a high pressure intensifier, hose system, nozzle holder, nozzle and x-y-z-positioning table. The experimental setup is shown in Fig. 3. The experimental conditions are listed in Table 2. One specimen of every mixture was subjected to the water jet by cutting five parallel kerfs on the top surface. The length of each kerf was 11.0 cm and the distance between the single kerfs was 5.0 mm. The specimens were placed inside a closed plexiglas cell so that it was possible to collect the removed material, which was collected and dried for 24 hours at room temperature. Two examples are shown in Fig. 4. These samples were weighed to estimate the amount of removed material, and the grain size distributions were estimated by sieve analysis using a conventional sieve shaker. Additionally, selected samples of the removed material were observed by optical microscopy.

Wear Particle Size Analysis

Figure 5 shows the grain size distributions of the removed wear particle samples. Based on these results, the specific surface and the average grain diameter of the particle samples were estimated. The specific surface was calculated according to Eq. [2] given in Ref. (*14*) for the estimation of the surfaces of comminution products:

$$S_{SP} = \frac{6}{\psi} \cdot \frac{\int_{d_U}^{d_0} d^2 f(d)\,dd}{\int_{d_U}^{d_0} d^3 f(d)\,dd} \qquad [2]$$

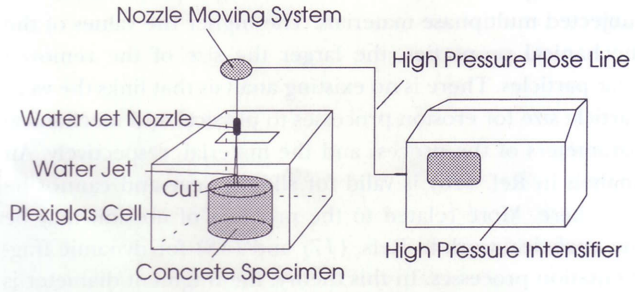

Fig. 3—Experimental setup.

TABLE 2—EXPERIMENTAL CONDITIONS

PARAMETER	UNIT	VALUE
Pump pressure	MPa	250
Flow velocity	m/s	670
Nozzle diameter	mm	0.23
Standoff distance	mm	15
Exposure time	min	92

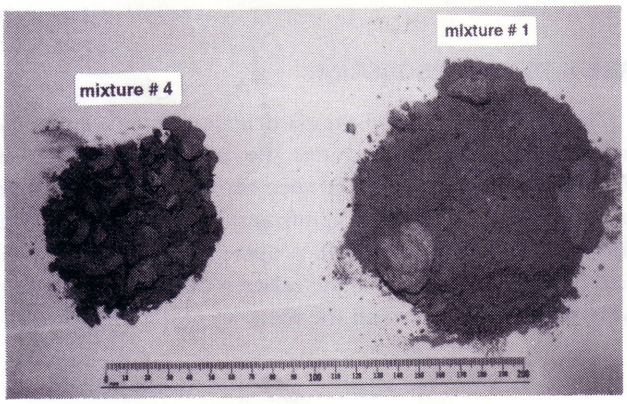

Fig. 4—Concrete wear particle samples after collecting and drying (scale in mm).

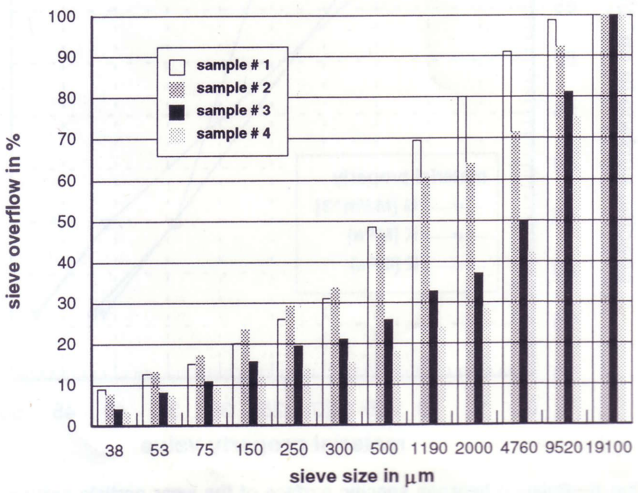

Fig. 5—Sieve analysis of the collected concrete wear particle samples.

Here, S_{SP} is the specific surface of the grain sample, d is the sieve width, and d_U and d_0 are the minimum sieve width and the maximum sieve width, respectively. The parameter ψ is a shape number which is assumed here as $\psi = 1$ for spheres. The integrals are solved by a commercial PC-program.

The average wear particle diameter was defined in this study as a "Sauter Diameter" and calculated using the following equation (*14*):

$$d_{AV} = \frac{6 \cdot V_M}{\rho_M \cdot S_{SP}} \quad [3]$$

Here, d_{AV} is the average particle diameter of the grain sample, V_M is the removed material volume, and ρ_M is the density of the specimen material as given in Table 1. For further evaluation, the results of Eq. [2] were used to calculate the specific crack lengths using Eq. [4] derived by Ref. (*15*) for mineral fragmentation processes:

$$l_{cr} = \sqrt{\frac{1}{2} \cdot S_{SP}} \quad [4]$$

Here, l_{cr} is the specific crack length. The results of Eqs. [2]–[4] are the basis for the evaluation of the investigated wear particle samples.

RESULTS AND DISCUSSION

The specific surfaces of the particle samples, estimated using Eq. [4], are plotted against the material properties in Fig. 6. The differences in the specific surface of the certain particle samples are not significant. The specific surface drops with increasing strength properties. This trend is verified by Fig. 7, which shows the relation between the average wear particle diameter and the material properties. The particle diameter increases with higher values of the mechanical parameters, suggesting that larger particles tend to be removed from the samples with the higher strengths. The diameter values are much lower than particle diameters for concrete erosion by water flow with velocities up to 350 m/s (*5*). One reason may be the fact that the Rosin-Rammler-Sperling (RRSB) grain size distribution used in Ref. (*5*) is characterized by an average diameter d' which does not have the same meaning as the average diameter used in the present study. It was not possible to fit the grain size measurements of this study by a straight line in the RRSB diagram. Another problem may be related to the different flow conditions in both investigations; Ref. (*5*) used a comparatively large water flow nozzle (diameter 1.0 mm). The specific crack lengths, calculated using Eq. [4], are shown in Fig. 8. The measured values are similar to that reported for the comminution of cement clinker ($l_{cr} = 8$ cm/cm^3) (*15*). The specific crack length is reduced for the materials with higher strength parameters. This is in agreement with the larger wear particle diameters for these materials.

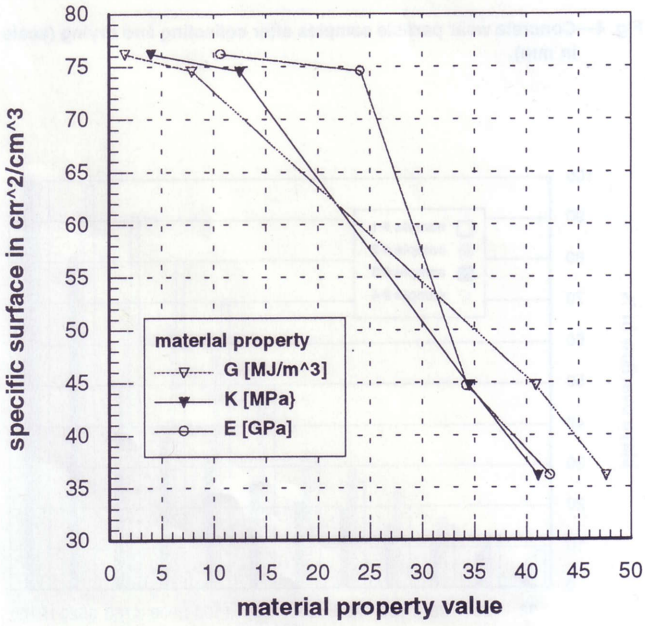

Fig. 6—Relation between specific surface of the wear particle samples and mechanical properties of the concrete mixtures.

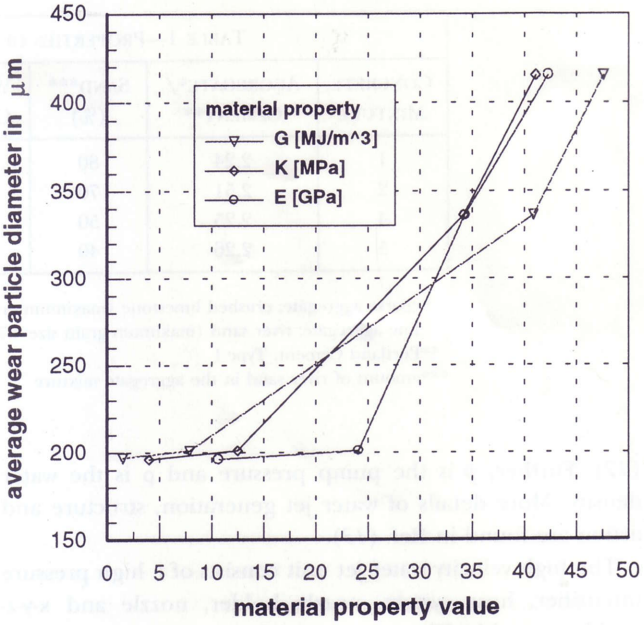

Fig. 7—Relation between the average wear particle diameter and mechanical properties of the concrete mixtures.

DISCUSSION

A significant relation exists between the size of the particles removed by erosive wear and the strength properties of the subjected multiphase materials. The higher the values of the mechanical properties, the larger the size of the removed wear particles. There is no existing analysis that links the wear particle size for erosion processes to physical and mechanical parameters of the process and the material, respectively. An analysis in Ref. (*16*) is valid for sliding wear and cannot be used here. More related to the problem of erosion may be the analytical work in Refs. (*17*) and (*18*) for dynamic fragmentation processes. In this theory, the fragment diameter is given by

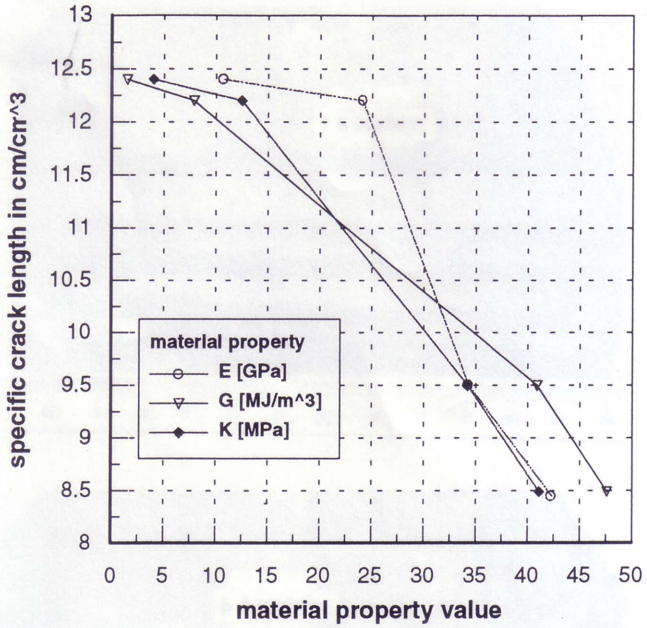

Fig. 8—Relation between specific crack length and mechanical properties of the concrete mixtures.

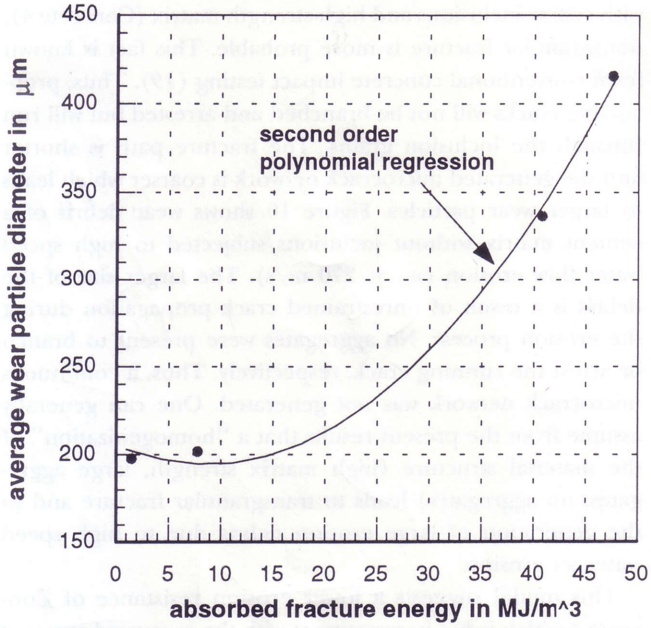

Fig. 9—Relation between measured average wear particle diameter, calculated average particle wear diameter,and the absorbed fracture energy of the concrete mixtures.

$$d_{AV} = 2 \cdot 5^{1/3} \cdot \left[\frac{K_{lc}}{\rho_M \cdot C_M \cdot \dot{\varepsilon}}\right]^{2/3} \quad [5]$$

Here, K_{lc} is the fracture toughness of the target material, ρ_M is the density of the target material, C_M is the wave velocity of the target material, and $\dot{\varepsilon}$ is the applied strain rate. This equation does not agree with the experimental results given in Fig. 6, which shows that the average wear particle diameter increases with Young's modulus. Young's modulus is quadratic proportional to the wave velocity in the material. It can also be seen from Table 1 that the average wear particle size increases with the density of the material.

Therefore, a regression analysis was carried out considering the influence of the compressive strength, the absorbed fracture energy, Young's modulus, and the material density on the average wear particle diameter. The results of the regression analysis are listed in Table 3. The absorbed fracture energy shows the best fit for all selected regressions. The best fit ($R^2 = 0.998$) was found for a polynomial regression between the wear particle diameter and the absorbed fracture energy as given in Eq. [6]:

$$d_{AV}(G) = a \cdot G^2 + b \cdot G + c \quad [6]$$

where a, b, and c are the regression parameters, as shown in Table 3. The results of Eq. [6] are plotted against the measured values in Fig. 9. This result has to be discussed with some caution because only four experimental points are estimated and because it suggests a minimum wear particle diameter at a certain value of the absorbed fracture energy (in Fig. 9, $G_{MIN} = 10$ MJ/m^3). However, the good fits of the absorbed fracture energy, and also of the compressive strength, suggest that the fracture processes occurring during the compression test of the samples are related to the material removal process due to high speed water flow erosion.

Based on the short review given in the introduction, it may be useful to relate the different wear particle sizes to different conditions for crack propagation in the materials. The more dense the generated microcrack network, the smaller the created wear particles may be. It can be assumed for the fine-grained material with a low-strength matrix (Concrete 1) that the cracks follow the interfaces between matrix and aggregates or will be branched and arrested by the aggregate grain. The fracture is mainly intergranular. This may lead to the generation of an extensive dense microcrack network. This assumption is verified experimentally by the comparatively high specific crack length in this material. In the material

TABLE 3—REGRESSION COEFFICIENTS (R^2) OF THE REGRESSION ANALYSIS FOR $d_{AV} = f$(MATERIAL PROPERTY)

REGRESSION TYPE	REGRESSION EQUATION	MATERIAL PROPERTY			
		COMPRESSIVE STRENGTH	YOUNG'S MODULUS	ABSORBED ENERGY	DENSITY
Linear	$a + b \cdot x$	0.973	0.921	0.977	0.859
Parabolic	$a \cdot x^b$	0.899	0.847	0.900	0.837
Polynomial	$a \cdot x^2 + b \cdot x + c$	0.995	0.984	0.998	0.861
Logarithmic	$a + b \cdot lnx$	0.882	0.836	0.883	0.858
Exponential	$a \cdot b^x$	0.982	0.924	0.989	0.836

with coarse inclusions and high-strength matrix (Concrete 4), transgranular fracture is more probable. This fact is known from conventional concrete impact testing (*19*). Thus, propagating cracks will not be branched and arrested but will run through the inclusion grains. The fracture path is shorter and the generated microcrack network is coarser which leads to larger wear particles. Figure 10 shows wear debris of a cement matrix without inclusions subjected to high speed water flow erosion (v_{fl} = 270 m/s). The larger size of the debris is a result of unrestrained crack propagation during the erosion process. No aggregates were present to branch or arrest the running crack, respectively. Thus, a continuous microcrack network was not generated. One can generally assume from the present results that a "homogenization" of the material structure (high matrix strength, large aggregates, no aggregates) leads to transgranular fracture and to the generation of large erosion debris due to high speed water jet erosion.

This model suggests a lower erosion resistance of Concrete 4 which is not in agreement with the measured material removal rates. The reason for this disagreement may be the higher specific surface energy of the inclusions which is more than two orders of magnitude higher than those of the matrix-aggregate interface. It was observed during conventional concrete testing that the work of fracture increases with increasing aggregate size (*20*), (*21*). The high amount of energy which is absorbed from the crack penetrating through the aggregate may explain the lower material removal rates for the high-strength material with the high strength matrix and the larger inclusion size.

These assumptions are supported by observations of the erosion sites. As Fig. 11 shows, a high amount of fractured aggregate grains exist in Concrete 4, whereas the erosion site of Concrete 1 is characterized by about 100% undamaged aggregate grains. Figure 12(a) shows a detail of Concrete 1 after the erosion. Here, the process of "washing out" the small aggregate grains, which means a failure path along the interface between matrix and aggregate grain, is clearly illustrated. Figure 12(b) is more typical for the erosion behavior of Concrete 4 containing coarser aggregates. The figure shows a large aggregate grain fractured by the high speed water flow.

Fig. 10—Photograph of wear debris of plain cement matrix subjected to high speed water flow (scale in mm).

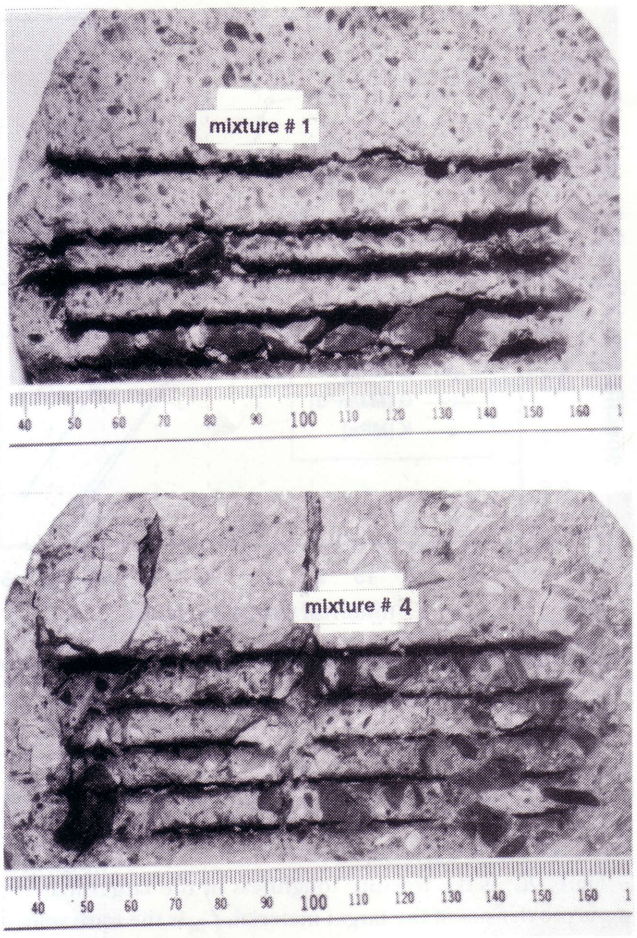

Fig. 11—Photographs from the erosion sites of two concrete mixtures. The dark small lines running from left-to-right are the generated kerfs. Note some fractured areas in the upper picture and the undamaged aggregate grains in the lower kerf of the lower picture (scales in mm).

The general idea presented above gets some additional support from erosion measurements carried out by Momber (*22*), who found an increasing aggregate fracture probability in concretes eroded by water jets with increasing loading rate. This was attributed to the observation that an increase in the stress rate leads to a homogenization of the concrete structure, as observed during conventional high rate loading of concrete (*23*).

SUMMARY

The results of this study can be summarized as follows. The relation between the size of the wear particles generated during the high speed water jet erosion and conventional mechanical properties of concrete was investigated. It was found that every concrete mixture is characterized by a certain average wear particle diameter. The average wear particle diameter tends to increase with increasing strength properties of the investigated materials. The average wear particle di-

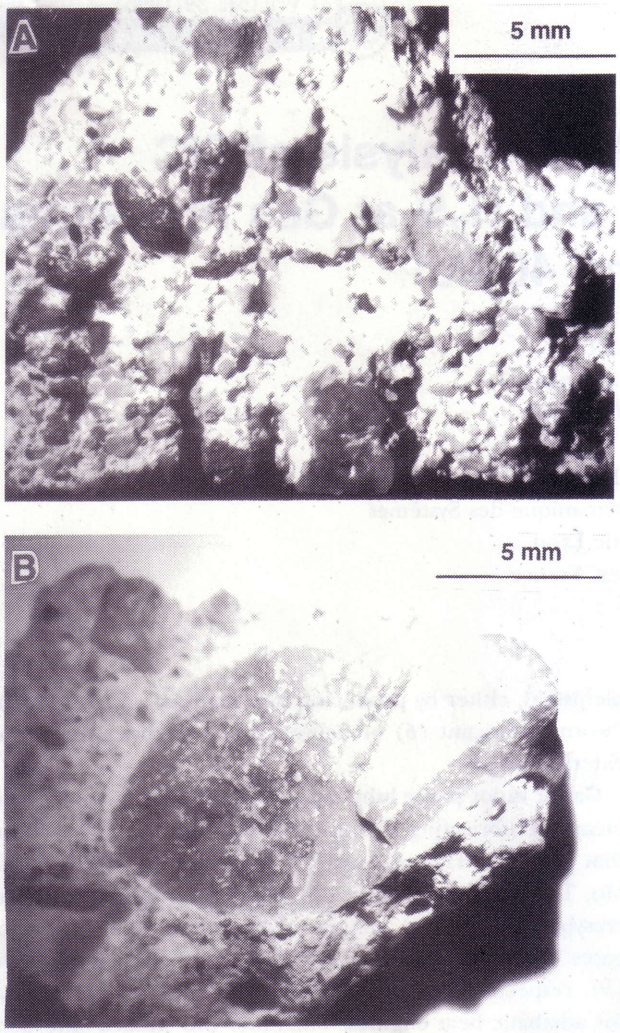

Fig. 12—Optical micrographs of the erosion sites of different concrete mixtures.
(a) Mixture No. 1: note the undamaged aggregate grains remained in the structure after the erosion process (magnification: 1:6)
(b) Mixture No. 4: note the brittle fracture of the large aggregate grain (magnification: 1:6)

ameter shows the best fit to the energy absorbed during the concrete compression test. A preliminary model is proposed that links the wear particle size with the structure of the microcrack network generated during the erosion process. As a general conclusion, it is suggested that the size of the eroded wear particles depends on the *length* of the microcrack network, whereas the erosion intensity (material removal rate) is determined by the *paths* of the cracks.

ACKNOWLEDGMENTS

The authors express gratitude to the Alexander-von-Humboldt Foundation, Bonn, Germany, and the Center for Robotics and Manufacturing Systems at the University of Kentucky, Lexington, KY, for financial support. Thanks is also addressed to Mr. D. Hunsacker, Kentucky Transportation Center, for testing the specimens, and to Mr. R. Schünemann and Mr. D. Pfeiffer for carrying out part of the experimental work.

REFERENCES

(*1*) Davies, A. P., "Save Velocities of Wear in Concrete," *Eng. News,* **22,** pp 20–21, (1912).
(*2*) Price, W. H., "Erosion of Concrete by Cavitation and Solids in Flowing Water," *Jour. of the ACI Proc.,* **43,** pp 1009–1023, (1947).
(*3*) Momber, A. and Kovacevic, R., "Fundamental Investigations on Concrete Wear by High Velocity Water Flow," *Wear,* **177,** pp 55–62, (1994).
(*4*) Momber, A., Kovacevic, R. and Ye, J., "The Fracture of Concrete Due to Erosive Wear by High Velocity Water Flow," *Trib. Trans.,* **38,** pp 686–692, (1995).
(*5*) Momber, A., "Investigations in the Behavior of Concrete Due to Water Jet Attack," *VDI Forschungsheffe,* No. 109, pp 1–137, (1992), (in German).
(*6*) Momber, A., "Mercury Intrusion Porosimetry Measurements on Concrete Samples Subjected by Water Jets," *Materialwiss. und Werkstofft.,* **42,** pp 283–286, (1992), (in German).
(*7*) Momber, A. and Louis, H., "On the Behavior of Concrete under Water Jet Impingement," *Mat'l. and Struct.,* **27,** pp 153–156, (1994).
(*8*) Momber, A. and Kovacevic, R., "Removal of Brittle Multiphase Materials by High Energy Water Jet," *Jour. Mat'l. Sci.,* (1995).
(*9*) Momber, A. and Kovacevic, R., "The Influence of Material Instabilities in a Brittle Multiphase Material on its Behavior in High Energy Water Jet Machining," *AMD-Vol.* **183**/ *MD-Vol.* **50,** pp 327–344, (1994).
(*10*) Momber, A. and Kovacevic, R., "Statistical Character of the Failure of Multiphase Materials Due to High Pressure Water Jet Impingement," *Int'l. Jour. of Fracture,* **71,** pp 1–14, (1995).
(*11*) Roylance, B. L. and Raadnui, S., "The Morphological Attributes of Wear Particles—Their Role in Identifying Wear Mechanisms," *Wear,* **175,** pp 115–121, (1994).
(*12*) Momber, A. and Kovacevic, R., "Energy Dissipative Processes in High Speed Water-Solid Particle Erosion," *Int'l. Forum on Measurement Techniques in Multiphase Flows,* Paper No. **M1,** (1995).
(*13*) Momber, A., *Manual of Pressurized Water Jets,* Beton-Verlag, Düsseldorf, (1993), (in German).
(*14*) Schubert, H., *Mineral Processing,* **1,** Verlag für Grundstoffind., Leipzig, Germany, (1988), (in German).
(*15*) Bond, F. C., "Evaluation of Fine Particle Grinding," *Aufber. Techn.,* **5,** pp 211–218, (1964).
(*16*) Rabinowicz, E. and Foster, R. G., "Effect of Surface Energy on the Wear Process," *ASME Jour. Basic Eng.,* **93,** pp 306–312, (1964).
(*17*) Glenn, L. A., Gommerstadt, B. T. and Chudnovsky, A., "A Fracture Mechanics Model of Fragmentation," *Jour. Appl. Phys.,* **60,** pp 1224–1226, (1986).
(*18*) Grady, D. E., "Local Inertial Effects in Dynamic Fragmentation," *Jour. Appl. Phys.,* **53,** pp 322–325, (1982).
(*19*) Reinhardt, H. W., "Concrete Under Impact Loading, Tensile Strength and Bond," *Heron,* **27,** pp 5–41, (1982).
(*20*) Wittman, F. H., Rokugo, K., Brühwiler, E., Mihashi, H. and Simonin, P., "Fracture Energy and Strain Softening of Concrete as Determined by Means of Compact Tension Specimens," *Mat'l. and Struc.,* **21,** pp 21–32, (1988).
(*21*) Kleinschrodt, H. and Winkler, H., "The Influence of the Maximum Aggregate Size and the Size of Specimen on Fracture Mechanics Properties," in *Fracture Toughness and Fracture Energy,* Wittmann, F. H., ed., Elsevier, Amsterdam, pp 158–163, (1986).
(*22*) Momber, A., "Secondary Fragmentation in Water Jet Rock Cutting," *Int'l. Jour. Water Jet Tech.,* **2,** pp 52–55, (1994).
(*23*) Rossi, P., "A Physical Phenomenon Which Can Explain the Mechanical Behaviour of Concrete Under High Strain Rates," *Mat'l. and Struct.,* **24,** pp 422–424, (1991).